

# Generation of Scalar-Tensor Gravity Effects in Equilibrium State Boson Stars\*

G. L. Comer<sup>†</sup>

*Department of Science and Mathematics, Parks College of Engineering and Aviation  
Saint Louis University, P.O. Box 56907, St. Louis, MO 63156-0907, USA*

Hisao Shinkai<sup>‡</sup>

*Department of Physics, Washington University, St. Louis, MO 63130-4899, USA  
(September 25, 1997 (revised version))*

Boson stars in zero-, one-, and two-node equilibrium states are modeled numerically within the framework of Scalar-Tensor Gravity. The complex scalar field is taken to be both massive and self-interacting. Configurations are formed in the case of a linear gravitational scalar coupling (the Brans-Dicke case) and a quadratic coupling which has been used previously in a cosmological context. The coupling parameters and asymptotic value for the gravitational scalar field are chosen so that the known observational constraints on Scalar-Tensor Gravity are satisfied. It is found that the constraints are so restrictive that the field equations of General Relativity and Scalar-Tensor Gravity yield virtually identical solutions. We then use catastrophe theory to determine the dynamically stable configurations. It is found that the maximum mass allowed for a stable state in Scalar-Tensor Gravity in the present cosmological era is essentially unchanged from that of General Relativity. We also construct boson star configurations appropriate to earlier cosmological eras and find that the maximum mass for stable states is smaller than that predicted by General Relativity, and the more so for earlier eras. However, our results also show that if the cosmological era is early enough then only states with positive binding energy can be constructed.

PACS number(s): 04.40.-b, 04.40.Dg, 04.50.+h

## I. INTRODUCTION

General Relativity describes very well the gravitational interaction. However, it still has competitors, one of which is Scalar-Tensor Gravity (see Will [1] for a review). Besides the metric, Scalar-Tensor Gravity has an additional scalar field. Motivation for this additional field can be found in Dicke's [2] discussions about arbitrariness in the measurement of lengths, times, and masses. There is also the fact that dilaton gravity is the low string tension limit of string theory (see, for instance, Damour and Polyakov [3]). Motivation for the theory itself, is the attractor mechanism discussed by Damour and Nordtvedt [4] (see also [5,6]). They demonstrate that the homogeneous and isotropic expansion of the universe forces a series of Scalar-Tensor cosmological solutions to be virtually indistinguishable from General Relativity solutions at late cosmological times. This implies that today the weak-field differences between Scalar-Tensor Gravity and General Relativity are small. It is the purpose here to see if significant strong-field differences between the two can be generated for equilibrium state boson stars.

A boson star consists of massive scalar particles (i.e., excitations of a complex scalar field) that are held together by gravity, a self-interaction, or both. They were first discussed by Kaup [7] and then by Ruffini and Bonazzola [8] (for a thorough review, see Liddle and Madsen [9]). They can form stable configurations having negative binding energy. If we include a self-interaction, then their maximum allowed stable mass comes to the order of a solar mass [10]. It is even speculated that they are a form of dark matter and that they can be created during a phase transition in the early universe (see Frieman et al [11]). Unlike boson stars formed today, those formed in the early universe would have done so in an era when even the weak-field differences between Scalar-Tensor Gravity and General Relativity are significant.

In terms of their equilibrium characteristics, there are infinitely many different boson star configurations for a given central density, depending on how many nodes, or zeroes, there are in the matter scalar field. Furthermore, the ground state, or zero-node configuration, has the lowest ADM mass, the higher-node configurations then have successively higher masses. With this in mind, there are three different ways that we try to generate non-trivial

---

\*gr-qc/9708071, To appear in *Classical and Quantum Gravity*.

<sup>†</sup>Email: [comergl@pxa.slu.edu](mailto:comergl@pxa.slu.edu)

<sup>‡</sup>Email: [shinkai@wurel.wustl.edu](mailto:shinkai@wurel.wustl.edu)

Scalar-Tensor effects: (i) build zero- and higher-node configurations for three different values of the matter scalar field self-interaction, (ii) build sequences of zero-node solutions, where different sequences have different values for the self-interaction, and (iii) repeat (i) and (ii) for two different Scalar-Tensor theories.

The two varieties of Scalar-Tensor Gravity considered here use the linear Brans-Dicke coupling [12] and the quadratic coupling used by Damour and Nordtvedt [4]. Experiments performed in our solar system have placed a lower bound on the slope of the Brans-Dicke linear coupling [1]. We will only consider Brans-Dicke boson stars that are consistent with this lower bound. As for the quadratic coupling, we impose boundary conditions such that the gravitational scalar can have an asymptotic value equal to the ambient, cosmological value existing at the present time, as well as earlier times. The ambient value is derived from a cosmological solution that exhibits the attractor mechanism of Damour and Nordtvedt [4]. When the present-day ambient value is used, then the present-day observational constraints are satisfied.

Boson stars in Scalar-Tensor Gravity have been investigated previously by Gundersen and Jensen [13], who used the Brans-Dicke [12] coupling, and by Torres [14], who looked at three different classes of couplings. Both discussions considered only zero-node configurations. Here we will consider solutions containing up to two nodes. Furthermore, neither of the previous discussions considered the question of stability. Here, we will apply catastrophe theory to the binding energy to determine the change of stability for the zero-node solutions. Finally, we, like Torres, will look at boson stars formed in earlier eras of the history of the universe.

We will show below that stable, zero-node boson star solutions in Scalar-Tensor Gravity are, for all practical purposes, indistinguishable from those of General Relativity in the present cosmological era. We also show that the same holds for the higher-node solutions, regardless of the strength of the self-interaction. It is for this reason that we construct zero-node boson star configurations appropriate to earlier cosmological eras, so as to determine if the indistinguishability of the solutions is a generic feature of boson stars or a consequence of the cosmological conditions. We shall see that it is the cosmology that is predominate, in agreement with the suggestion of Torres [14] that masses can decrease from their General Relativity values for earlier cosmological eras. But moreover, we use catastrophe theory to show that the maximum, stable mass decreases as the cosmological time decreases. However, when the cosmological era is early enough, we find that only positive binding energies result so that no stable configuration can be constructed.

The fact that negative binding energy states can exist at all is a priori a non-trivial result. Such states can be realized within General Relativity [17] because a boson star's typical mass is  $M \sim 1/Gm$  and its total number of particles is  $N_p \sim 1/Gm^2$ —where  $G$  is the Newton gravitational coupling and  $m$  is the individual mass of the scalar particles making up the star—and so both are of comparable value in the binding energy  $M - mN_p$ . However, one way in which Scalar-Tensor Gravity differs from General Relativity is in how it locally varies the Newton gravitational coupling (see, for instance, Bekenstein [18] and Bekenstein and Meisels [6], and references therein). The inherent non-linear features of the Scalar-Tensor field equations suggest that a spatially varying  $G$ , which at a very basic level controls the strength of the gravitational interaction between two particles, should lead to qualitative differences in binding energy between General Relativity and Scalar-Tensor Gravity. We shall derive below a necessary condition for negative binding energies to exist.

In the next section we will introduce the field equations for the gravitational fields and the matter. In Sec. III we write down the equations in spherically symmetric form. Similar to the approach of Friedberg et al [19], we write down a total energy functional from which the field equations can be derived. It is also here that we discuss the boundary conditions and the numerical technique. In Sec. IV we give a detailed account of the solutions containing up to two nodes for a typical central value of the matter scalar field. In Sec. V, we investigate the stability of the ground state configurations through the use of catastrophe theory. In Sec. VI we discuss boson stars formed in earlier cosmological eras. Finally, in Sec. VII we make some concluding remarks. Units such that  $c = 1$  and  $\hbar = 1$  will be used. This implies that the scalar field mass  $m$  is an inverse length (actually, the inverse Compton wavelength of the scalar particles) and the bare gravitational constant  $G_*$  has units of length squared.

## II. THE FIELD EQUATIONS

The action for our system of Scalar-Tensor Gravity coupled to a self-interacting, complex scalar field in the physical, “Jordan-frame” is

$$S = \frac{1}{16\pi} \int d^4x \sqrt{-\tilde{g}} \left[ \phi \tilde{R} - \phi^{-1} \omega(\phi) \tilde{g}^{\mu\nu} \partial_\mu \phi \partial_\nu \phi \right] - \int d^4x \sqrt{-\tilde{g}} \left[ \frac{1}{2} \tilde{g}^{\mu\nu} \partial_\mu \psi^\dagger \partial_\nu \psi + \left( \frac{m^2}{2} \psi^\dagger \psi + V(\psi^\dagger \psi) \right) \right] + B.T. , \quad (2.1)$$

where  $B.T.$  represents the boundary terms that can be added to subtract out the second-order derivatives coming from  $R$  [20,21] (the explicit form being identical to that used by Friedberg et al [19] and will be given below in the “Einstein-frame”). The gravitational scalar is  $\phi$  and  $\omega(\phi)$  is the “Jordan-frame” coupling of  $\phi$  to the matter. The complex scalar  $\psi$  (with its complex conjugate being  $\psi^\dagger$ ) has mass  $m$  and is self-interacting through the potential  $V(\psi^\dagger\psi)$ .

There is an alternative representation of the action above, for the so-called “Einstein-frame.” The transition to this frame is effected by the conformal transformation

$$\tilde{g}_{\mu\nu} = e^{2a(\varphi)} g_{\mu\nu} , \quad (2.2)$$

where

$$\phi^{-1} = G_* e^{2a(\varphi)} \quad (2.3)$$

and  $a(\varphi)$  is the functional transformation from  $\phi$  to the “Einstein-frame” gravitational scalar  $\varphi$ . The relationship between  $\omega(\phi)$  and  $a(\varphi)$  is obtained from

$$\alpha^2 = (2\omega + 3)^{-1} , \quad (2.4)$$

where

$$\alpha(\varphi) \equiv \frac{\partial a}{\partial \varphi} . \quad (2.5)$$

The action in the “Einstein-frame” is thus

$$S = \frac{1}{16\pi G_*} \int d^4x \sqrt{-g} [R - 2g^{\mu\nu} \partial_\mu \varphi \partial_\nu \varphi - \int d^4x \sqrt{-g} \left[ \frac{1}{2} e^{2a(\varphi)} g^{\mu\nu} \partial_\mu \psi^\dagger \partial_\nu \psi + e^{4a(\varphi)} \left( \frac{m^2}{2} \psi^\dagger \psi + V(\psi^\dagger \psi) \right) \right] + B.T. . \quad (2.6)$$

It does not deliver exactly General Relativity because the metric  $g_{\mu\nu}$  is not the true, physical metric that encodes the distance between spacetime points. However, the “Einstein-frame” does deliver equations that are similar enough to General Relativity that we will use it for our calculations.

The “Einstein-frame” stress-energy tensor is

$$T_{\mu\nu} = \frac{1}{2} e^{2a(\varphi)} (\partial_\mu \psi^\dagger \partial_\nu \psi + \partial_\nu \psi^\dagger \partial_\mu \psi) - \frac{1}{2} e^{2a(\varphi)} \left( \partial_\tau \psi^\dagger \partial^\tau \psi + e^{2a(\varphi)} [m^2 \psi^\dagger \psi + 2V(\psi^\dagger \psi)] \right) g_{\mu\nu} . \quad (2.7)$$

The gravitational field equations for  $g_{\mu\nu}$  and  $\varphi$  are

$$G_{\mu\nu} = 8\pi G_* T_{\mu\nu} + 2\partial_\mu \varphi \partial_\nu \varphi - \partial_\tau \varphi \partial^\tau \varphi g_{\mu\nu} \quad (2.8)$$

and

$$\nabla_\sigma \nabla^\sigma \varphi = -4\pi \alpha T , \quad (2.9)$$

where  $T$  is the trace of the stress-energy tensor. The matter field equations are

$$\nabla_\sigma \nabla^\sigma \psi^\dagger + 2\alpha \partial_\tau \psi^\dagger \partial^\tau \varphi = e^{2a(\varphi)} \left( m^2 \psi^\dagger + 2 \frac{\partial V}{\partial \psi} \right) \quad (2.10)$$

and

$$\nabla_\sigma \nabla^\sigma \psi + 2\alpha \partial_\tau \psi \partial^\tau \varphi = e^{2a(\varphi)} \left( m^2 \psi + 2 \frac{\partial V}{\partial \psi^\dagger} \right) . \quad (2.11)$$

The coupling function  $a(\varphi)$  is a priori unknown. There are, however, some theoretical reasons to motivate explicit forms. Furthermore, once a particular form for  $a(\varphi)$  is taken, there are experimental constraints [1,22] that can be imposed (using Eqs. (3.18) and (3.19) below). The two forms for  $a(\varphi)$  that will be used here are the Brans-Dicke coupling

$$a(\varphi) = \frac{\varphi - \varphi_\infty}{\sqrt{2\omega_{BD} + 3}} \quad (2.12)$$

and the quadratic coupling

$$a(\varphi) = \frac{1}{2}\kappa(\varphi^2 - \varphi_\infty^2) , \quad (2.13)$$

which was the particular form considered by Damour and Nordtvedt [4] (except for the additive constant). The term  $\varphi_\infty$  represents the asymptotic value of the gravitational scalar field. It is known from Solar System observations that  $\omega_{BD} > 500$ ; likewise, it is known from observations of binary pulsars that  $\kappa > -5$  [22].

As for the complex scalar field, we will be considering a self-interaction of the form

$$V(\psi^\dagger\psi) = \frac{\Lambda}{4}(\psi^\dagger\psi)^2 . \quad (2.14)$$

The strength of the self-interaction,  $\Lambda$ , will be taken to be positive. Because the potential  $V(\psi^\dagger\psi)$  is a functional of  $\psi^\dagger\psi$  then it preserves the global U(1) gauge symmetry ( $\psi \rightarrow e^{i\sigma}\psi$ , where  $\sigma$  is a constant) present in the theory. This symmetry results in a conserved current, whose explicit form in the “Jordan-frame” is

$$\tilde{J}^\mu = \frac{i}{2}e^{-2a(\varphi)}g^{\mu\nu}(\psi\partial_\nu\psi^\dagger - \psi^\dagger\partial_\nu\psi) . \quad (2.15)$$

This conserved current leads to a conserved charge, which is  $N_p$ , the number of particles making up the star (cf., Eq. (3.11) below).

### III. THE EQUILIBRIUM STATE EQUATIONS

#### A. The equilibrium state field equations

The spacetimes considered here are spherically symmetric and static, with the “Einstein-frame” metric taking the form

$$ds^2 = -N^2(r)dt^2 + A(r)dr^2 + r^2[d\theta^2 + \sin^2\theta d\phi^2] . \quad (3.1)$$

The gravitational scalar, which is real, is assumed also to be spherically symmetric and static:

$$\varphi = \varphi(r) . \quad (3.2)$$

As for the matter scalar field, Friedberg et al [19] show that the minimum energy configurations are those for which

$$\psi = e^{-i\Omega t}\Phi(r) , \quad (3.3)$$

where  $\Omega$  is real and positive. Their proof (see the Appendix in [19]) also goes through for scalar-tensor gravity (making use of an energy functional defined as below in Eq. (3.10)), and so we will take  $\psi$  to have this form.

To write down the field equations for this system we could take Eqs. (3.1-3.3) and insert them into the full field equations written earlier. However, it is more useful to insert Eqs. (3.1-3.3) directly into Eq. (2.6), and then derive the field equations from the reduced action. Let  $L_{matter}$  represent the reduced “matter” Lagrangian (which includes the contribution due to  $\varphi$ ),  $L_{grav}$  the reduced gravitational Lagrangian, and  $L = L_{matter} + L_{grav}$  the total Lagrangian, i.e.,  $S = \int dt L$  where  $S$  is the total reduced action. Then for our particular system we find

$$L_{matter} = -\frac{m^2}{G_*} \int_0^\infty dr r^2 N\sqrt{A}(u + v - w) \quad (3.4)$$

and

$$L_{grav} = \frac{1}{2G_*} \int_0^\infty dr N \left( \sqrt{A} - 2 \left[ 1 + r \frac{N'}{N} \right] + \frac{1}{\sqrt{A}} \left[ 1 + 2r \frac{N'}{N} \right] \right) , \quad (3.5)$$

where

$$w = \frac{2\pi G_* \Omega^2}{m^2 N^2} e^{2a(\varphi)} \Phi^2 , \quad (3.6)$$

$$u = 2\pi G_* \left( 1 + \frac{\Lambda}{2m^2} \Phi^2 \right) e^{4a(\varphi)} \Phi^2 , \quad (3.7)$$

and

$$v = \frac{1}{2m^2 A} \left( 4\pi G_* e^{2a(\varphi)} [\Phi']^2 + [\varphi']^2 \right) . \quad (3.8)$$

Note that the gravitational Lagrangian does *not* follow just from the Hilbert action, it also includes the contributions due to the boundary term *B.T.* of Eq. (2.6):

$$B.T. = \frac{1}{4G_*} \left( \int dt \left[ \frac{2Nr^2}{\sqrt{A}} \left( \frac{N'}{N} + \frac{2}{r} \right) - 4Nr \right] \right) \Big|_{r=0}^{r=\infty} . \quad (3.9)$$

We can obtain the total energy functional  $E$  (i.e., Hamiltonian) from the Lagrangian via the standard canonical transformation that replaces  $\dot{\psi}$  with its conjugate momentum:

$$\begin{aligned} E &= \Omega N_p - L \\ &= \frac{m^2}{G_*} \int_0^\infty dr r^2 N \sqrt{A} (w + u + v) - L_{grav} , \end{aligned} \quad (3.10)$$

where  $N_p$  is the conserved total particle number (in the physical “Jordan-frame”) and is given by

$$N_p = \frac{2m^2}{G_* \Omega} \int_0^\infty dr r^2 N \sqrt{A} w . \quad (3.11)$$

By construction it is the case that

$$\Omega = \left[ \frac{\partial E}{\partial N_p} \right]_{\Phi, \varphi, A, N} = \frac{dM}{dN_p} , \quad (3.12)$$

where  $M$  is the “on-shell” total mass-energy (given below in Eq. (3.20)), and  $N_p$  is also “on-shell.”

There are now two ways to derive the field equations: one can vary  $L$  keeping  $\Omega$  fixed to get them, or one can vary  $E$  keeping  $N_p$  fixed. Either way gives the same results, which are

$$\frac{A'}{A} = \frac{1-A}{r} + 2m^2 r A (w + u + v) , \quad (3.13)$$

$$\frac{2N'}{N} = -\frac{1-A}{r} + 2m^2 r A (w - u + v) , \quad (3.14)$$

$$\left( \frac{r^2 N \varphi'}{\sqrt{A}} \right)' = 4\pi G_* m^2 r^2 N \sqrt{A} e^{2a(\varphi)} \alpha \left( \left[ 2e^{2a(\varphi)} - \frac{\Omega^2}{m^2 N^2} \right] \Phi^2 + \frac{1}{Am^2} [\Phi']^2 + \frac{\Lambda}{m^2} e^{2a(\varphi)} \Phi^4 \right) , \quad (3.15)$$

and

$$\left( \frac{r^2 N e^{2a(\varphi)} \Phi'}{\sqrt{A}} \right)' = m^2 r^2 N \sqrt{A} e^{2a(\varphi)} \left( e^{2a(\varphi)} - \frac{\Omega^2}{m^2 N^2} \right) \Phi + \lambda r^2 N \sqrt{A} e^{4a(\varphi)} \Phi^3 . \quad (3.16)$$

## B. Boundary conditions

The boundary conditions for this system of equations must take into account three things: (i) the solutions must be geometrically regular at the origin; (ii) the solutions must yield an asymptotically flat spacetime; and (iii) the solutions must take into account the cosmological input for both the coupling  $a(\varphi)$  as well as  $\varphi$ .

Geometrical regularity at the origin means there is no conical singularity, i.e., the proper radius divided by the proper circumference should reduce to  $2\pi$  at  $r = 0$ . This implies that  $A(0) = 1$ . Also, to maintain regularity in the field equations as  $r \rightarrow 0$ , we impose that  $\Phi'(0) = 0$  and  $\varphi'(0) = 0$ .

For a purely technical reason (to be discussed below), we desire solutions that are asymptotically flat in both the Jordan and Einstein frames. That is, we want both  $\tilde{g}_{\mu\nu}$  and  $g_{\mu\nu}$  to reduce to the flat spacetime metric at spatial infinity. The implication of this is that the value of  $\varphi_\infty \equiv \varphi(\infty)$  must be such that  $a(\varphi_\infty) = 0$ . The other outcome is that both  $N$  and  $A$  approach one at spatial infinity.

For the Brans-Dicke coupling,  $\Phi_c \equiv \Phi(0)$  and  $\varphi_\infty$  are the only freely specified field values. The value of  $N(0)$  is not specified freely, but rather is determined so that  $\Phi_\infty \equiv \Phi(\infty) = 0$ . The value of  $\varphi$  at the origin is not specified freely; it must be determined in such a way that the solution for  $\varphi$  goes to  $\varphi_\infty$  at spatial infinity. We will use the freedom to add an arbitrary constant to the Brans-Dicke coupling  $a(\varphi)$  (to be discussed in more detail below) so that all the solutions we consider have  $\varphi_\infty = 0$ .

For the quadratic coupling, again  $\Phi_c$  can be specified freely, but we use the cosmological model of Damour and Nordtvedt [4] to calculate  $\varphi_\infty$ , i.e.,

$$\varphi_\infty \sim \frac{\alpha_R}{\kappa} \left(1 - \frac{3}{8\kappa}\right)^{-1/2} e^{-3p/4} \sin \left( \frac{3}{4} \sqrt{\frac{8\kappa}{3} - 1} p + \arctan \sqrt{\frac{8\kappa}{3} - 1} \right), \quad (3.17)$$

where  $\alpha_R \sim 1$  is the value of  $\alpha$  for the universe at the end of the radiation dominated era and  $p$  is a measure of the time since this era (i.e., today,  $p \sim 10$ ); in terms of the cosmological redshift  $z$  we have  $z \sim e^{10-p} - 1$ . Note that we must take  $\kappa \equiv \partial\alpha/\partial\varphi > 3/8$ .

Damour and Nordtvedt used a form of the scalar-tensor coupling without an additive constant (cf. Eq. (2.13)). Fortunately, it can be shown that putting in such a constant does not change the solution above for  $\varphi_\infty$ . Furthermore, the addition of such a constant will not affect the predictions of Damour and Nordvedt for the PPN (Parametrized Post-Newtonian) parameters  $\gamma - 1$  and  $\beta - 1$  or the time rate-of-change of the Newton coupling, since each of these only depend on the present day values for  $\alpha$  and  $\kappa$ :

$$\gamma - 1 = -\frac{2\alpha^2}{1 + \alpha^2} \quad (3.18)$$

and

$$\beta - 1 = -\frac{1}{8}\kappa(\gamma + 1)(\gamma - 1). \quad (3.19)$$

Observational constraints (see Will [1], and references therein) yield  $|\gamma - 1| < 2 \times 10^{-3}$  and  $|\beta - 1| < 2 \times 10^{-3}$ .

## C. ADM Mass

A consequence of determining  $\varphi$  at spatial infinity such that  $a(\varphi_\infty) = 0$  is that the ADM mass  $M$  is given by

$$G_* M = m^2 \int_0^\infty dr \, r^2 (w + u + v). \quad (3.20)$$

This can be shown as follows: the “Jordan-frame” ADM mass  $M_J$  is given by

$$G_* M_J = \lim_{r \rightarrow \infty} \frac{r}{2} (1 - 1/\tilde{g}_{rr}). \quad (3.21)$$

The similar “Einstein-frame” ADM mass  $M_E$  is

$$G_* M_E = \lim_{r \rightarrow \infty} \frac{r}{2} (1 - 1/g_{rr}). \quad (3.22)$$

However, since  $\tilde{g}_{rr} = e^{2a(\varphi)} g_{rr}$  and  $a(\varphi_\infty) = 0$ , then the limits on the right-hand-sides are equal and therefore  $M_J = M_E \equiv M$ . Eq. (3.20) follows using the integrated form of Eq. (3.13). Furthermore, it can be shown that the value for  $M$  one obtains from Eq. (3.20) is the same as that delivered by the “on-shell” value for the total energy functional  $E$  of Eq. (3.10).

#### D. Necessary condition for negative binding energy states

If the condition

$$2 > \Omega/m \quad (3.23)$$

is satisfied, then negative binding energy states can be constructed. This can be established by first adding together Eqs. (3.13) and (3.14), which results in

$$(\ln [N^2 A])' = 4m^2 r A(v + w) . \quad (3.24)$$

The right-hand-side of this equation is positive-definite so that  $(\ln [N^2 A])' > 0$  for all  $r$ . Our choice of coordinates and boundary conditions dictate that

$$\lim_{r \rightarrow \infty} \ln (N^2 A) = 0 . \quad (3.25)$$

Therefore,  $\ln (N^2 A) < 0$  for all finite  $r$  and thus  $N^2 A < 1$ . Because the integrand of  $M$  is positive definite (for positive  $\Lambda$ ), and  $N\sqrt{A} < 1$  in the integrand for  $N_p$ , then

$$mN_p < 2(m/\Omega)M . \quad (3.26)$$

Now, a negative binding energy state is defined by the condition  $M - mN_p < 0$ . Using the inequality in Eq. (3.26) we see  $M < mN_p < 2(m/\Omega)M$ , and hence the result in Eq. (3.23) follows.

Actually, the preceding discussion does not give the tightest limit on the ratio  $\Omega/m$ . An even tighter constraint on  $\Omega/m$  can be found by looking at the asymptotic form for  $\Phi$  as  $r$  gets very large. In this limit, the field equation for  $\Phi$  becomes (assuming also that  $\Phi^3$  is negligible compared to  $\Phi$ )

$$\Phi'' - (m^2 - \Omega^2) \Phi \approx 0 , \quad (3.27)$$

the solution of which is  $\Phi \sim \exp(-\sqrt{m^2 - \Omega^2} r)$ . Thus, the stronger constraint is that  $\Omega/m < 1$ .

#### E. Rescaled equations

We will take advantage of scale-invariances of the field equations to redefine some of the fields, parameters, and the radial and time coordinates:

$$x = mr , \sqrt{4\pi G_*} \Phi \rightarrow \Phi , mN/\Omega \rightarrow N , \Lambda/4\pi G_* m^2 \rightarrow \Lambda , \Omega t/m \rightarrow t . \quad (3.28)$$

The field equations become (' =  $d/dx$ )

$$\frac{A'}{A} = \frac{1 - A}{x} + 2xA(w + u + v) , \quad (3.29)$$

$$\frac{2N'}{N} = -\frac{1 - A}{x} + 2xA(w - u + v) , \quad (3.30)$$

$$\left( \frac{x^2 N \varphi'}{\sqrt{A}} \right)' = x^2 N \sqrt{A} e^{2a(\varphi)} \alpha \left( \left[ 2e^{2a(\varphi)} - N^{-2} \right] \Phi^2 + \frac{1}{A} [\Phi']^2 + \lambda e^{2a(\varphi)} \Phi^4 \right) , \quad (3.31)$$

$$\left( \frac{x^2 N e^{2a(\varphi)} \Phi'}{\sqrt{A}} \right)' = x^2 N \sqrt{A} e^{2a(\varphi)} \left( e^{2a(\varphi)} - N^{-2} \right) \Phi + \Lambda x^2 N \sqrt{A} e^{4a(\varphi)} \Phi^3 , \quad (3.32)$$

where now

$$w = \frac{1}{2N^2} e^{2a(\varphi)} \Phi^2 , \quad (3.33)$$

$$u = \frac{1}{2} \left( 1 + \frac{\Lambda}{2} \Phi^2 \right) e^{4a(\varphi)} \Phi^2 , \quad (3.34)$$

and

$$v = \frac{1}{2A} \left( e^{2a(\varphi)} [\Phi']^2 + [\varphi']^2 \right) . \quad (3.35)$$

The rescaling does not change the asymptotic value of  $A$ —it still becomes one at spatial infinity—but it does change that of  $N$ , which is now

$$\lim_{x \rightarrow \infty} N(x) = m/\Omega . \quad (3.36)$$

Thus boson stars with negative binding energies will have asymptotic values for (rescaled)  $N$  that will never be lower than 1. The total mass and total particle number are also changed to

$$M = \frac{1}{G_* m} \int_0^\infty dx x^2 (w + u + v) \sim \frac{1}{G_* m} \quad (3.37)$$

and

$$N_p = \frac{2}{G_* m^2} \int_0^\infty dx x^2 N \sqrt{A} w \sim \frac{1}{G_* m^2} . \quad (3.38)$$

The integrands, as well as the integrals themselves, are dimensionless. Hence, it is the factors in front that determine the typical values for  $M$  and  $N_p$ , and they are those discussed in the Introduction.

There is one more rescaling that can be done that has no analog in General Relativity, and that is an invariance of the field equations if an arbitrary constant is added to the scalar-tensor coupling. If we simultaneously do the rescaling

$$e^c x \rightarrow x , e^c \Phi \rightarrow \Phi , e^c N \rightarrow N , e^c \Lambda \rightarrow \Lambda \quad (3.39)$$

on the variables defined by Eq. (3.28) and let  $a(\varphi) + c \rightarrow a(\varphi)$ , then the field equations remain unchanged. It is for this reason that we can maintain all generality and still have boundary conditions for the universe today such that  $a(\varphi_\infty) = 0$ .

## F. Numerical technique

We have extended the code originally developed by Seidel and Suen [23] for General Relativity. It is based on a fourth-order Runge-Kutta algorithm and now solves the Scalar-Tensor Gravity differential equations (3.29)-(3.32). As mentioned earlier, our system requires a two parameter search to find a solution that satisfies the boundary conditions for  $\Phi_\infty$  and  $\varphi_\infty$  that were given earlier in Sec. III C. Operationally, we choose a central value of the scalar field  $\Phi_c$  first together with a guessed central value of the gravitational scalar field  $\varphi(0)$ , and integrate out to large radii for different values of  $N(0)$ . We then check if the resulting  $\varphi_\infty$  is close to our expected boundary value. In order to judge the convergence of the matter scalar field  $\Phi_\infty$ , we set the tolerance to  $10^{-10}$ , which means an asymptotic value for  $\Phi$  is convergent if it is less than this tolerance.

As readers will find later in Figs. 1-4, the gravitational scalar field falls off more slowly than the matter scalar field. The field equations (3.29)-(3.32) imply that the asymptotic behavior is  $\varphi \sim \varphi_\infty + C/x$ , where  $C$  is a constant. Therefore, at the numerical boundary, say  $x = x_{end}$ , we set the expected boundary values for  $\varphi(x_{end})$  as

$$\varphi(x_{end}) = \varphi_\infty + \frac{C}{x_{end}} , \quad (3.40)$$

where

$$C = -x_{end}^2 \left. \frac{d\varphi}{dx} \right|_{x=x_{end}} . \quad (3.41)$$

If the computed  $\varphi(x_{end})$  is not the expected value, then we change  $\varphi(0)$  and repeat the whole procedure. We set the tolerance to judge convergence in  $\varphi_\infty$  as  $5 \times 10^{-6}$ .

The key distinctions between the matter scalar field with no nodes, and one with nodes, is the zero-node field only has an extremum at the origin, and approaches zero asymptotically, whereas all higher-node solutions have as many new extrema as zeroes in the matter scalar field. Hence, the algorithm that constructs higher-node fields searches not only for zeroes, but also for local extrema. Convergence towards a solution satisfying the boundary conditions is effected by applying the same two tolerances given above. In particular, when we search for a solution having  $n$ -nodes, then we impose the tolerance after the matter scalar field has passed through the  $(n + 1)$ -th local minimum or maximum.

We have checked our code in three different ways: (i) Produced solutions in the large coupling limit and verified that they are identical with original General Relativity solutions; (ii) Replaced  $a(\varphi)$  with  $a(\varphi) + c$  and confirmed, for a given set of boundary conditions, that we obtain the same sequence of results; and (iii) Calculated the total mass  $M$  three different ways (using eqs. (3.20-3.22)) and obtained consistent results.

#### IV. THE EQUILIBRIUM CONFIGURATIONS

The main goal here is to see if significant Scalar-Tensor Gravity effects can be generated in equilibrium state boson stars. We strive for this goal in three ways: First, specific equilibrium configurations are constructed for a representative choice of the central value of the matter scalar field. We produce different configurations by increasing the node-number in the matter scalar field, increasing the strength of the matter scalar field self-interaction, or both. Second, we produce three sequences of zero-node configurations, where an individual member of a sequence is specified by the central value of the matter scalar field. The sequences themselves are distinguished by the strength of the matter scalar field self-interaction. Third, we repeat the previous two steps for the two different Scalar-Tensor couplings given in Eqs. (2.12-2.13) as well as for General Relativity.

We have in Figs. 1-3 typical plots of the radial dependence of the matter and gravitational fields for the Brans-Dicke coupling. Figs. 1a, 1b, and 1c contain plots of  $\Phi$  versus  $x$  for  $n = 0, 1, 2$ , where  $n$  represents the number of nodes in the matter scalar field, and  $\Lambda = 0, 10, 100$ . The corresponding plots for  $N$  and  $A$  are given in Figs. 2a, 2b, and 2c and those for  $\varphi$  in Figs. 3a, 3b, and 3c. All the configurations are for  $\Phi_c = 0.15$ , which will be seen in the next section to correspond to stable zero-node states, and  $\omega_{BD} = 600$ , which can be seen from Eq. (3.18) to be consistent with Solar System constraints. The same set of plots for boson stars in General Relativity are essentially indistinguishable from those presented here.

Notice that the effect of the nodes in the matter scalar field is to slightly flatten  $N$  in a small region around the  $x$  values where the nodes occur. For example, in Fig. 2c, we can see that  $A$  has two local extrema produced for each node in the scalar field. The local minimum occurs at precisely the value for  $x$  where the node occurs. The gravitational scalar  $\varphi$  behaves similarly to  $N$  near the nodes. This behaviour for each of the fields is a reflection of what is occurring in the energy density: it becomes nearly zero in the small region around each node. Thus, instead of the steady accumulation in mass that usually occurs as one moves radially outward from the center of a star, we have near each node essentially no accumulation. The metric function  $A(x)$ , for instance, then behaves like its black hole counterpart and decreases as a node is approached (since the mass enclosed within  $x$  remains nearly constant near each node). After passing through a node, the mass will start to accumulate again so  $A(x)$  will start to grow. Similar remarks apply to the other fields.

Initially, one might have expected the gravitational scalar field to have had some effect near the nodes. After all, the mass enclosed inside a given radius depends on the quantities  $w(x)$ ,  $u(x)$ , and  $v(x)$ . They, in turn, depend on the gravitational scalar field (cf., Eqs. (3.33)-(3.35)). It is because the gravitational scalar remains essentially constant (and that the realistic boundary conditions coming from the observational constraints force it to be small) that it has no significant effect on the accumulation of mass near the nodes. This, in turn, is due to the fact that the matter scalar field serves as a *direct* source for the gravitational scalar field (cf., Eq. (3.31)).

Using Tables I and II we can compare the masses, particle numbers, radii (which is defined to be the radial coordinate value from the star's center containing 95% of the mass), and central value for the lapse function  $N(0)$  between General Relativity and Brans-Dicke Gravity. Regardless of the node-number or value for  $\Lambda$ , there are essentially no differences between the two theories. If we take even larger values for  $\Lambda$  then the differences are even smaller. However, if we take smaller values for  $\omega_{BD}$  then the differences get bigger (see Ref. [13] for complete details on the  $n = 0$  case for  $\omega_{BD} = 6$ ). This increase is natural since it is well-known that smaller values of  $\omega_{BD}$  generally result in larger differences with General Relativity. It is thus not too surprising that when  $\omega_{BD} = 600$  we cannot generate significant Scalar-Tensor effects.

On the other hand, the quadratic coupling depends explicitly on the gravitational scalar field. Hence, even if the coupling is made to satisfy observational constraints at spatial infinity, it is still possible that the gravitational scalar can be made large enough inside a boson star that significant deviations from General Relativity can be produced.

We have constructed configurations for the quadratic coupling case with  $\kappa = 0.38$ , which is very close to the limiting value of  $\kappa = 3/8$  for this theory. Again, we take  $\Phi_c = 0.15$ . The quantitative results for  $\Phi$ ,  $N$  and  $A$  are virtually indistinguishable from the previous Brans-Dicke case, and thus General Relativity. The plot of the gravitational scalar  $\varphi$ , however, is different (see Figs. 4a, 4b, and 4c) in that it is positive, but still maintains the same basic shape as the Brans-Dicke case. The masses, particle numbers, radii, and central value for the lapse function  $N(0)$  for zero-, one-, and two-node solutions for  $\Phi_c = 0.15$  and  $\Lambda = 0, 10, 100$  are listed in Table III. Comparison with the previous two tables shows no important differences in any of the values. Also, if we take larger values of  $\kappa$  the differences are even smaller than those for  $\kappa = 0.38$ . It is because the observational constraints force the gravitational scalar to be small at spatial infinity that this coupling is unable to generate any significant differences with General Relativity. That is we see in Figs. 4a-c that the field equations are able to change the gravitational scalar by factors of order unity, but not factors of, say, a hundred.

The second way in which we are to extract differences between General Relativity and Scalar-Tensor Gravity is to consider sequences of zero-node configurations, where individual members in a sequence are delimited by their value for  $\Phi_c$ . In Fig. 5 we have a plot of  $M, N_p$  vs  $\Phi_c$ , for  $\Lambda = 0, 10, 100$ . For each value of  $\Lambda$  we see that there is an absolute maximum mass, and number of particles, that any boson star can have, exactly as in General Relativity. (Similar results for the mass were obtained by Gunderson and Jensen [13] for the Brans-Dicke coupling with  $\omega_{BD} = 6$ , as well as the couplings considered by Torres [14].) Not unexpected, the value for the maximum mass and particle number are not changed significantly from the General Relativity results. In Fig. 6 we have plots of the binding energy versus the particle number. We note that all branches starting from  $\Phi_c = 0$  have negative binding energies, just like General Relativity. The corresponding plots for the quadratic coupling (for  $p = 10$ , and  $\kappa = 0.38$ ) contain essentially the same features as Brans-Dicke Gravity.

So, we see that the observational constraints are so restrictive that no significant deviations from General Relativity can be produced. However, we can at least extract some generic behaviour pertinent to the gravitational scalar, and for boundary conditions consistent with observational constraints, from Figs. 7 and 8. They are the Brans-Dicke and quadratic coupling graphs, respectively, of  $M$  vs  $\varphi(0)$  for a sequence of zero-node configurations having  $\Lambda = 0, 10, 100$ . Each curve is parameterized by  $\Phi_c$ , and starts at  $M = 0$ . As  $\Phi_c$  gets bigger, then  $\varphi(0)$  decreases and  $M$  increases. At precisely the same value of  $\Phi_c$  where the maximum mass occurs,  $M$  reaches its maximum value in Figs. 7 and 8; also, the local minimum  $M$  in both Figs. 7 and 8 corresponds to the first local minimum in Fig. 5.

The first point to be grasped from these plots is that the central value of the gravitational scalar has an absolute minimum value. The second is that there is a region of the graph where the same value for  $\varphi(0)$  corresponds to two different mass values. There is even the “crossover” point where two configurations have exactly the same mass. (It can be inferred from the discussion below that one configuration is stable, and the other is not.) The final point is that there is the asymptotic region where the mass  $M$  oscillates slightly in value, but  $\varphi(0)$  continues to grow. This is certainly surprising, since one would expect a growing  $\varphi(0)$  (which is related to the Newton gravitational coupling between two particles) to force the mass to change monotonically.

## V. STABILITY ANALYSIS VIA CATASTROPHE THEORY

Catastrophe theory is a relatively new mathematical tool to explain a variety of changes of state in physical systems [15]. Rigorous theorems have been established demonstrating its validity. It is particularly adept at extracting discontinuous changes of state when gradual changes occur in the system parameters. It has been used in General Relativity to analyze the stability of black holes [24], non-abelian black holes [25], and boson stars [16]. Most importantly for the present work, is that application of catastrophe theory to boson stars [16] delivers the same results for changes in stability that are obtained from dynamical, numerical analysis [23].

Catastrophe theory can be used to determine stability if the system under analysis develops bifurcations, or cusps, when curves existing in its so-called equilibrium space are projected into its lower-dimensional control parameter space. The variables for the equilibrium space are given by a *potential function*, *control parameters*, and *state variables*. The variables for the control parameter space are the potential function and the control parameters. For the problem at hand, the equilibrium space is three-dimensional and the control parameter space two-dimensional, with the binding energy  $M - mN_p$  taken to be the potential function, the total particle number  $N_p$  chosen to be the control parameter, and the central value of the matter scalar field  $\Phi_c$  taken to be the state variable. An equivalent variation on this choice for the equilibrium space and the control parameter space is to replace the total particle number with the mass.

The appearance of a cusp in a curve’s projection is not enough to determine a change in stability. Rather, if it is known that a system is stable along one branch of a curve in the control parameter space, then it will become unstable on the next branch formed at a cusp. The trick is in determining stability along the previous branch. Like the case of General Relativity [16], we can assume that boson stars along the very first branches in Fig. 6 (i.e., those

that start at  $N_p = 0$  and end at the cusp labeled  $B_1$ ) are stable. They are the only ones composed entirely of negative binding energy states, they contain the flat-space limit, and furthermore, results of a dynamical, numerical analysis demonstrate that they are stable against small perturbations [26].

Fig. 9 is the typical equilibrium space for the Brans-Dicke coupling. The projection into the  $(N_p, \Phi_c)$  plane at  $M - mN_p = 0$  gives the same curve for the particle number as in Fig. 5. The projection into the  $(N_p, M - mN_p)$  plane at the maximum  $\Phi_c$  value gives the same curve as in Fig. 6. It is this second projection that yields the control parameter space. Hence, the cusp labeled  $B_1$  in Fig. 6 represents a change in stability, since the configurations on the branch leading up to  $B_1$  are all stable. At the cusp we have  $\Phi_c = 0.09$  and a mass of  $M = 2.255/G_*m$ , which is not significantly different from the corresponding General Relativity result (see [16]). The cusp at  $B_2$  does not represent a change in stability since the binding energies near this point are positive; likewise, for the cusp at  $B_3$ . As one might expect, the maximum stable masses for  $\Lambda = 0$  and 10 are not significantly different from their General Relativity values. Neither are the quadratic coupling results, since the equilibrium space and control parameter space are virtually identical to what is depicted in Fig. 9.

## VI. CONFIGURATIONS IN THE EARLIER UNIVERSE

We have seen that the attractor nature to General Relativity of the quadratic model extends also to a sequence of equilibrium boson star configurations. Therefore, we repeat here the same calculations as the previous section but for earlier eras for the universe according to the quadratic coupling model. Going to earlier eras means taking smaller values for  $p$  (which, recall, is related to the redshift via  $z \sim e^{10-p} - 1$ ) in Eq. (3.17). Our interest will be focused on the maximum allowed stable mass.

A not so trivial point is that all our calculations must be made within the *same* Scalar-Tensor theory. What this means is that we are allowed to choose the additive constant to the coupling function  $a(\varphi)$  only once, and not change it when we change the value for  $p$ . We will stick with the choice that makes  $a(\varphi_\infty) = 0$  at  $p = 10$ . Thus,  $a(\varphi_\infty)$  is not zero for any other value of  $p$ . This complicates the determination of the ADM mass, since for  $p \neq 10$  it can no longer be obtained from Eq. (3.37). Fortunately, we can use the energy functional of Eq. (3.10) to determine the total mass, once the rescaling relations of Eqs. (3.28) and (3.39) are properly taken into account.

In Fig. 10 we have a plot of  $M$  vs  $\Phi_c$ . We only go far enough so that the first extremum can be clearly identified, which, as we know from the previous section, corresponds to the maximum stable mass. Clearly, the main effect is to decrease the mass, as suggested by Torres [14]. If we go to early enough cosmological eras ( $p < 5$ ), however, we find that the binding energy is positive, for all values of  $\Phi_c$  (see Fig. 11). Furthermore, the cusp that appears at  $B_1$  in Fig. 6 is clearly gone for  $p < 5$ . This indicates, then, that no stable Scalar-Tensor Gravity boson star can be formed during early enough cosmological times.

## VII. CONCLUDING REMARKS

The main point of this work is to see if significant Scalar-Tensor Gravity effects can be generated in equilibrium state boson stars, even when the fairly restrictive observational constraints are imposed. In contrast with earlier works [13,14], we constructed not only zero-node solutions, but also one- and two-node solutions. We also illustrated some of the interesting features of the gravitational scalar for the zero-node case, and used catastrophe theory to determine the maximum stable mass for the zero-node states. Finally, we confirmed Torres' [14] suggestion that masses decrease below corresponding General Relativity masses for boson stars formed in earlier eras of the history of the universe.

However, our results also show that stars formed too early are unstable. This suggests, for instance, that a scenario whereby boson stars are formed in some cosmological phase transition will not work in Scalar-Tensor Gravity. Moreover, there is every likelihood that *any* type of stellar object will suffer from the same instability. For instance, Harada [27] has recently shown that there are a range of values for the coupling for which perfect fluid stars are unstable, although no explicit connection with the ambient cosmological conditions is made.

We did not apply catastrophe theory to the higher-node solutions, because we know, from numerical evolutions [28], that they are all unstable in General Relativity. Dynamical 1-D evolutions are being performed to see if the higher-node solutions are generically unstable in Scalar-Tensor Gravity. As mentioned earlier, the code developed for these evolutions confirms that zero-node configurations on the initial branch of Fig. 6 are stable. It is also being investigated whether the zero-node states on the other branches collapse, or disperse. So far, the results do substantiate the conclusions obtained here using catastrophe theory. All these results are currently under preparation [26].

## ACKNOWLEDGMENTS

We thank Ed Seidel and Wai-Mo Suen for letting us modify their General Relativity boson star code [23] to Scalar-Tensor gravity, and Jay Balakrishna for pointing out subtleties in the higher-node algorithm. We also thank Wai-Mo Suen and Franz Schunck for useful conversations. H. S. was partially supported by the grant NSF PHYS 96-00507, 96-00049, and NASA NCCS 5-153.

---

- [1] C. M. Will, *Theory and experiment in gravitational physics* (Cambridge: Cambridge University Press, 1993).
- [2] R. H. Dicke, *Documents on Modern Physics: The Theoretical Significance of Experimental Relativity* (New York: Gordon and Breach, 1964), pp. 34-43.
- [3] T. Damour and A. M. Polyakov, Nuclear Physics **B423**, 532 (1994).
- [4] T. Damour and K. Nordtvedt, Phys. Rev. Lett. **70**, 2217 (1993); Phys. Rev. D **48**, 3436 (1993).
- [5] J. Garcia-Bellido, M. Quiros, Phys. Lett. B 243, 45 (1990).
- [6] J. D. Bekenstein and A. Meisels, Phys. Rev. D **18**, 4378 (1978).
- [7] D. J. Kaup, Phys. Rev. **172**, 1331 (1968).
- [8] R. Ruffini and S. Bonazzola, Phys. Rev. **187** (1969), 1767.
- [9] R. Liddle and M. S. Madsen, Int. J. Mod. Phys. D **1**, 101 (1992).
- [10] M. Colpi, S. L. Shapiro, and I. Wasserman, Phys. Rev. D **57**, 2485 (1986).
- [11] J. A. Frieman, G. B. Gelmini, M. Gleiser, and E. W. Kolb, Phys. Rev. Lett. **60**, 2101 (1988).
- [12] C. H. Brans and R. H. Dicke, Phys. Rev. **124**, 925 (1961).
- [13] M. A. Gunderson and L. G. Jensen, Phys. Rev. **D48**, 5628 (1993).
- [14] D. F. Torres, Phys. Rev. **D56**, 3478 (1997).
- [15] V. I. Arnol'd, *Catastrophe Theory* (Berlin: Springer-Verlag, 1992); T. Poston and I. Stewart, *Catastrophe Theory and Its Applications*, ( Pitman, London, 1978); R. Thom, *Strucure Stability and Morphogenesis*, (Benjamin, 1975).
- [16] F. V. Kusmartsev, E. W. Mielke and F. E. Schunck, Phys. Rev. **D43**, 3895 (1991), Phys. Lett. **A157**, 465 (1991); F. V. Kusmartsev and F. E. Schunck, Physica **B178**, 24 (1992).
- [17] W. Thirring, Phys. Lett. **127B**, 27 (1983).
- [18] J. D. Bekenstein, Phys. Rev. D **15**, 1458 (1977).
- [19] R. Friedberg, T. D. Lee, and Y. Pang, Phys. Rev. D **35**, 3640 (1987); ibid, 3658 (1987).
- [20] J. W. York, Phys. Rev. Lett. **28**, 1082 (1972).
- [21] G. W. Gibbons and S. W. Hawking, Phys. Rev. D **15**, 2753 (1977).
- [22] T. Damour and G. Esposito-Farèse, Phys. Rev. D **54**, 1474 (1996).
- [23] E. Seidel and W-M. Suen, Phys. Rev. **D42**, 384 (1990).
- [24] O. Kaburaki, I. Okamoto, and J. Katz, Phys. Rev. D **47**, 2234 (1993).
- [25] K. Maeda, T. Tachizawa, T. Torii, and T. Maki, Phys. Rev. Lett. **72**, 450 (1994).
- [26] J. Balakrishna and H. Shinkai, submitted to Phys. Rev. D., gr-qc/9712065; J. Balakrishna, G.L. Comer and H. Shinkai, in preparation.
- [27] T. Harada, Prog. Theo. Phys., **98**, 359 (1997).
- [28] J. Balakrishna, E. Seidel, and W-M. Suen, submitted to Phys. Rev. D., gr-qc/9712064.

$n$	$\Lambda$	$M$	$N_p$	$R$	$N(0)$	$m/\Omega$
0	0	0.5916	0.6056	8.760	0.8255	0.9210
	10	0.8573	0.8904	8.855	0.7628	0.8999
	100	1.963	2.034	9.485	0.4655	0.8575
1	0	1.288	1.316	18.34	0.8181	0.9482
	10	1.512	1.554	17.27	0.7723	0.9353
	100	2.531	2.612	14.09	0.4820	0.8881
2	0	1.983	2.025	28.26	0.8170	0.9636
	10	2.198	2.254	26.21	0.7756	0.9528
	100	3.112	3.199	19.20	0.4887	0.9007

TABLE I. Listed are some sample values for General Relativity, for ADM mass (modulo  $1/G_*m$ ), particle number (modulo  $1/G_*m^2$ ), radius (modulo  $1/m$ ), central value for  $N/(m/\Omega)$ , and  $m/\Omega$  for  $\Phi_c = 0.15$ .

$n$	$\Lambda$	$M$	$N_p$	$R$	$N(0)$	$m/\Omega$
0	0	0.5914	0.6021	8.750	0.8289	0.9247
	10	0.8571	0.8857	8.850	0.7679	0.9057
	100	1.964	2.026	9.475	0.4759	0.8765
1	0	1.288	1.312	18.32	0.8131	0.9424
	10	1.512	1.550	17.28	0.7671	0.9289
	100	2.531	2.604	14.08	0.4843	0.8921
2	0	1.983	2.020	28.25	0.8110	0.9564
	10	2.197	2.249	26.20	0.7686	0.9441
	100	3.113	3.192	19.20	0.4912	0.9051

TABLE II. Listed are some sample values for Brans-Dicke, for ADM mass (modulo  $1/G_*m$ ), particle number (modulo  $1/G_*m^2$ ), radius (modulo  $1/m$ ), central value for  $N/(m/\Omega)$ , and  $m/\Omega$  for  $\omega_{BD} = 600$  and  $\Phi_c = 0.15$ .

$n$	$\Lambda$	$M$	$N_p$	$R$	$N(0)$	$m/\Omega$
0	0	0.5916	0.6021	8.800	0.8271	0.9228
	10	0.8573	0.8856	8.875	0.7653	0.9029
	100	1.963	2.025	9.475	0.4681	0.8624
1	0	1.288	1.312	18.38	0.8128	0.9427
	10	1.512	1.550	17.30	0.7671	0.9290
	100	2.531	2.602	14.08	0.4842	0.8922
2	0	1.983	2.020	28.27	0.8068	0.9517
	10	2.198	2.245	26.22	0.7682	0.9438
	100	3.112	3.112	19.20	0.4861	0.8960

TABLE III. Listed are some sample values for the quadratic coupling, for ADM mass (modulo  $1/G_*m$ ), particle number (modulo  $1/G_*m^2$ ), radius (modulo  $1/m$ ), central value for  $N/(m/\Omega)$ , and  $m/\Omega$  for  $\kappa = 0.38$  and  $\Phi_c = 0.15$ .

## Figure captions

### Fig.1

Sample configurations of equilibrium state boson stars in the Brans-Dicke theory. Matter scalar field  $\Phi$  is plotted in the case of node=1 (a), 2 (b), and 3(c), respectively. Solid, dotted and three-dot-dash lines are for  $\Lambda = 0, 10$  and  $100$  case, respectively.

### Fig.2

Lapse  $N$  and the metric  $A$  for the solutions plotted in Fig.1. The lapse  $N$  has been re-scaled to its original form so that its asymptotic value is 1.

### Fig.3

Gravitational scalar field  $\varphi$  for the solutions plotted in Fig.1.

### Fig.4

Gravitational scalar field  $\varphi$  for the quadratic coupling model. The value for  $\Phi_c$  is the same as in Fig.1.

### Fig.5

Mass and particle numbers versus central matter scalar field in the Brans-Dicke theory.

### Fig.6

Binding energy  $M - mN_p$  versus particle number  $N_p$  in the quadratic coupling model.

### Fig.7

A sequence of equilibrium solutions in the Brans-Dicke theory. Mass versus central gravitational scalar field value is plotted.

### Fig.8

A sequence of equilibrium solutions in the quadratic coupling model. Mass versus central gravitational scalar field value is plotted.

### Fig.9

Equilibrium configurations in the equilibrium space. Binding energy  $M - mN_p$ , particle number  $N_p$  and the center matter scalar field  $\Phi_c$  are taken as the potential function, control parameter, and state parameter, respectively. One equilibrium sequence line and three projected lines of it onto 2-parameter planes are shown. The plot on the  $(N_p, M - mN_p)$  plane is identical with Fig.6.

### Fig.10

Changing the boundary condition for  $\varphi_\infty$  via the cosmological solution of the quadratic coupling. The sequences of equilibrium solutions for cosmological time parameter  $p = 10$ (solid line), 6(three-dots-dash line) and 5(dotted line) are plotted. The solid lines are identical with those in Fig.5.

### Fig.11

Binding energy vs. particle number  $N_p$  for different cosmological time  $p = 10, 9, \dots, 1$ . The case for  $p = 10$  is the same as Fig.6. Only the range  $0 \leq \Phi_c \leq 0.5$  is plotted.

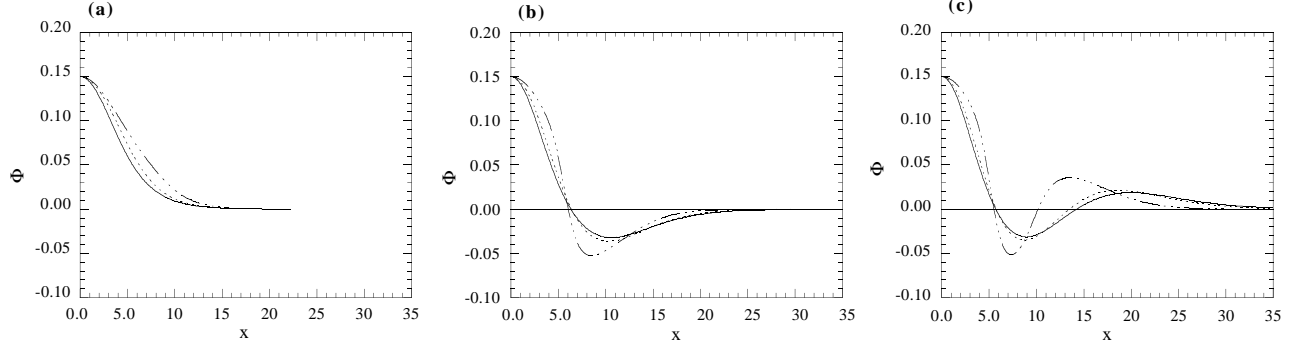


FIG. 1. Sample configurations of equilibrium state boson stars in the Brans-Dicke theory. Matter scalar field  $\Phi$  is plotted in the case of node=1 (a), 2 (b), and 3(c), respectively. Solid, dotted and three-dot-dash lines are for  $\Lambda = 0, 10$  and  $100$  case, respectively.

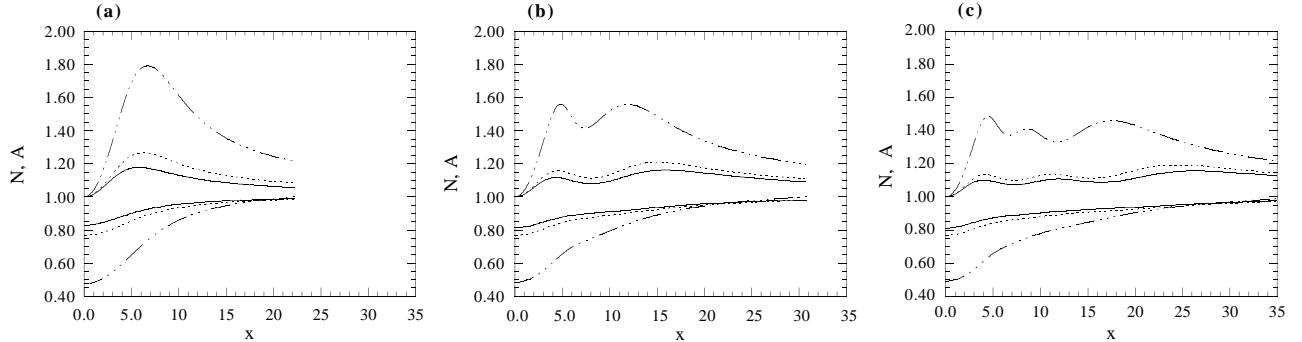


FIG. 2. Lapse  $N$  and the metric  $A$  for the solutions plotted in Fig.1. The lapse  $N$  has been re-scaled to its original form so that its asymptotic value is 1.

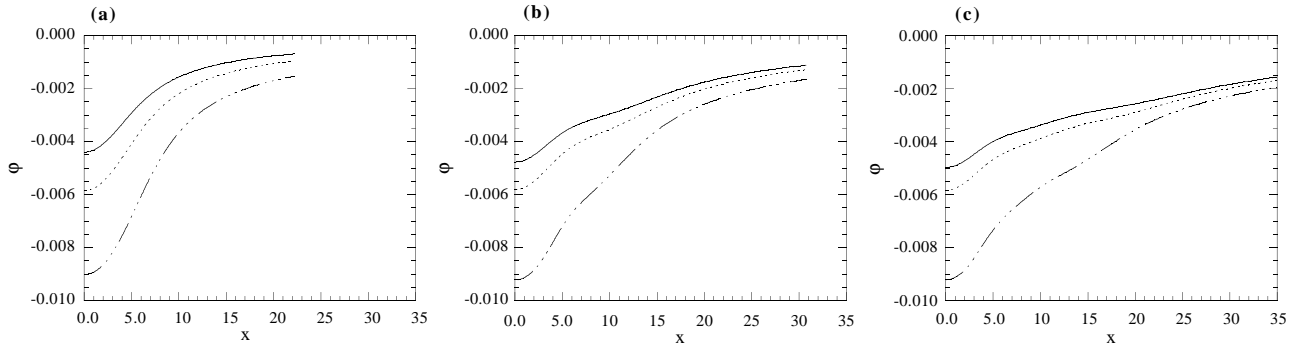


FIG. 3. Gravitational scalar field  $\varphi$  for the solutions plotted in Fig.1.

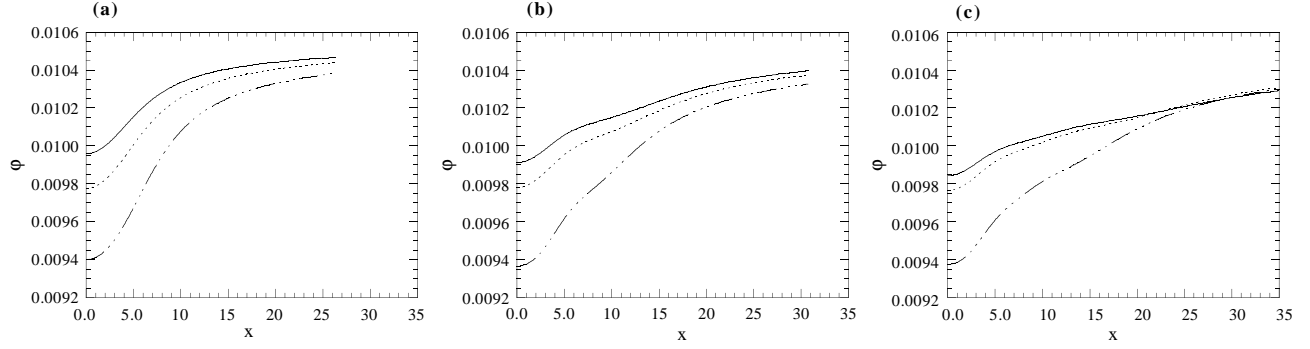


FIG. 4. Gravitational scalar field  $\varphi$  for the quadratic coupling model. The value for  $\Phi_c$  is the same as in Fig.1.

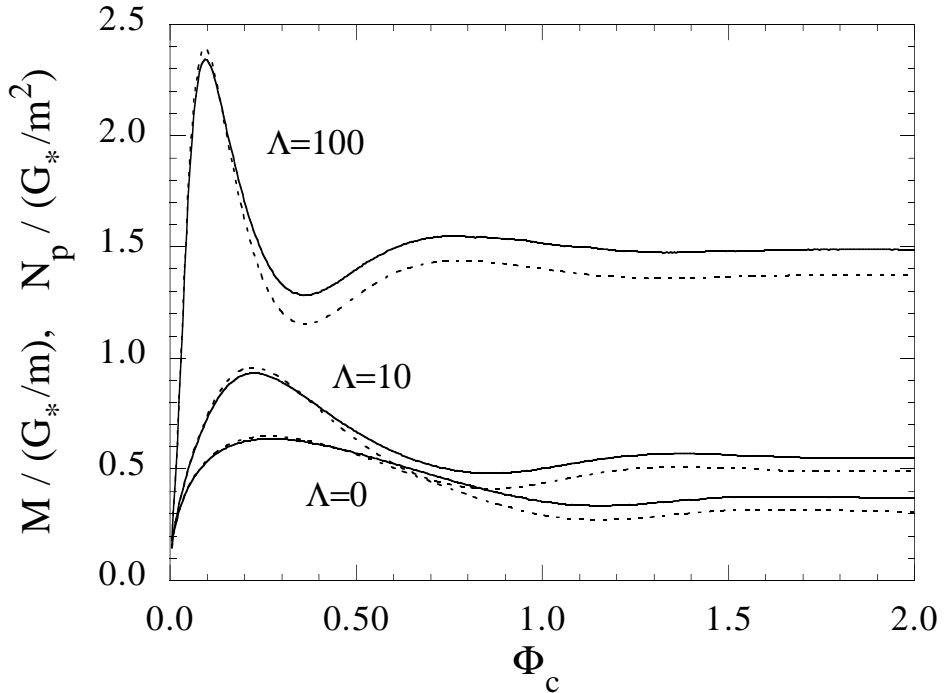


FIG. 5. Mass and particle numbers versus central matter scalar field in the Brans-Dicke theory.

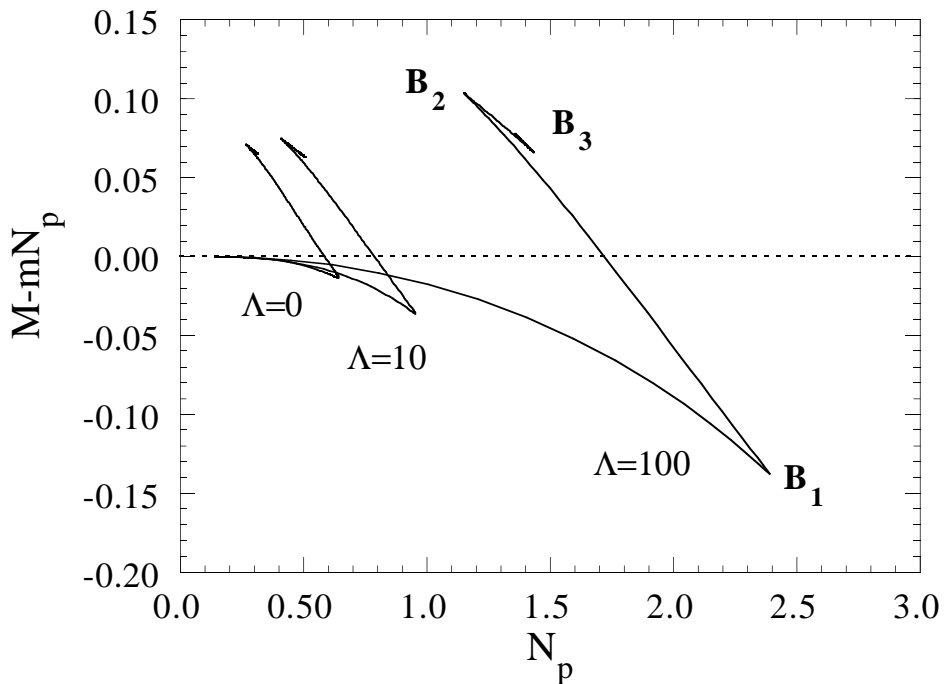


FIG. 6. Binding energy  $M - mN_p$  versus particle number  $N_p$  in the quadratic coupling model.

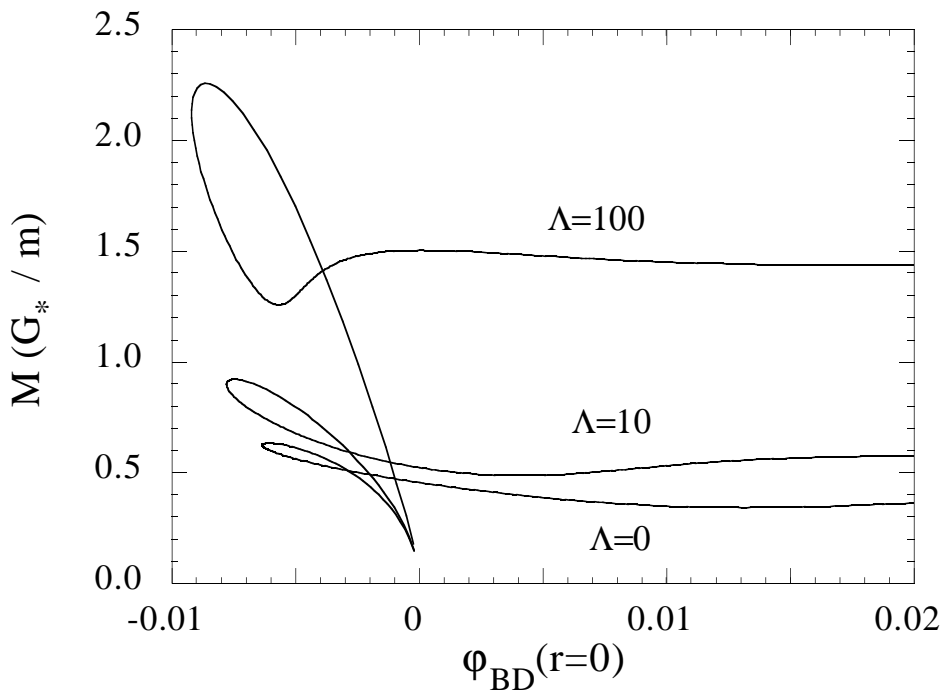


FIG. 7. A sequence of equilibrium solutions in the Brans-Dicke theory. Mass versus central gravitational scalar field value is plotted.

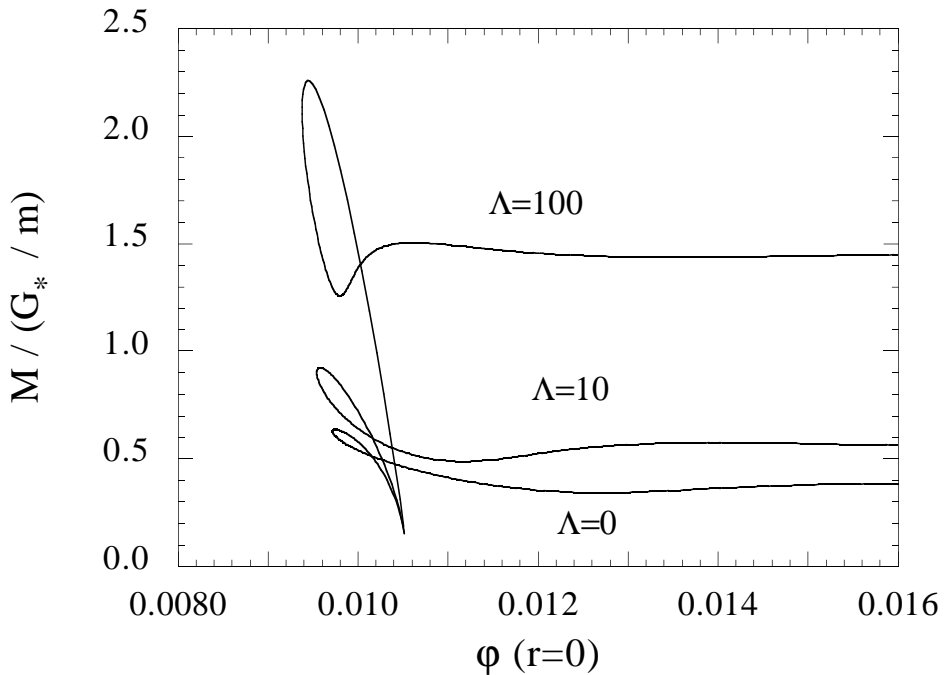


FIG. 8. A sequence of equilibrium solutions in the quadratic coupling model. Mass versus central gravitational scalar field value is plotted.

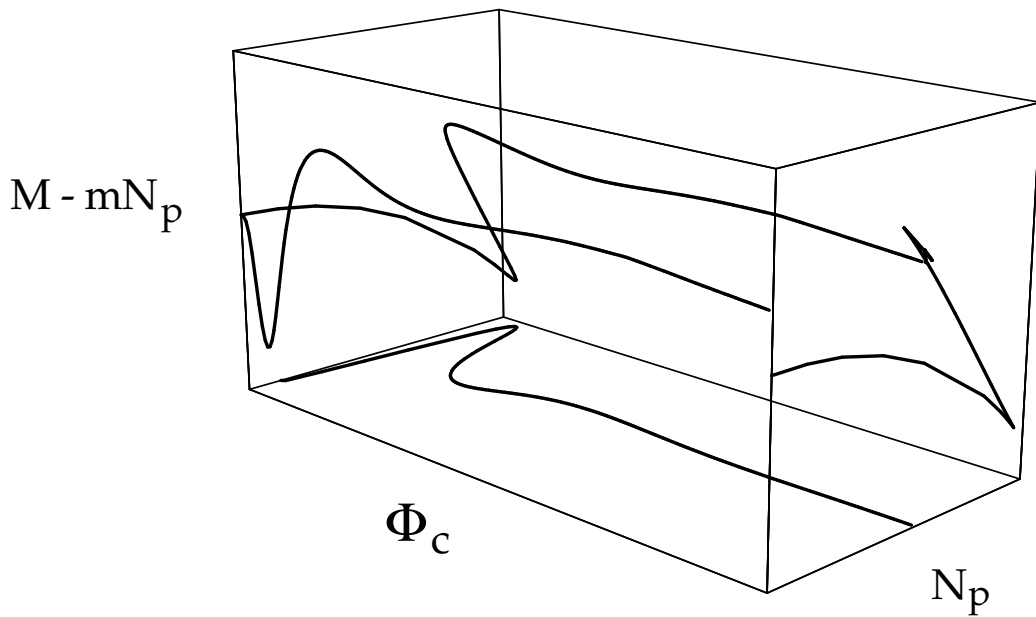


FIG. 9. Equilibrium configurations in the equilibrium space. Binding energy  $M - mN_p$ , particle number  $N_p$  and the center matter scalar field  $\Phi_c$  are taken as the potential function, control parameter, and state parameter, respectively. One equilibrium sequence line and three projected lines of it onto 2-parameter planes are shown. The plot on the  $(N_p, M - mN_p)$  plane is identical with Fig.6.

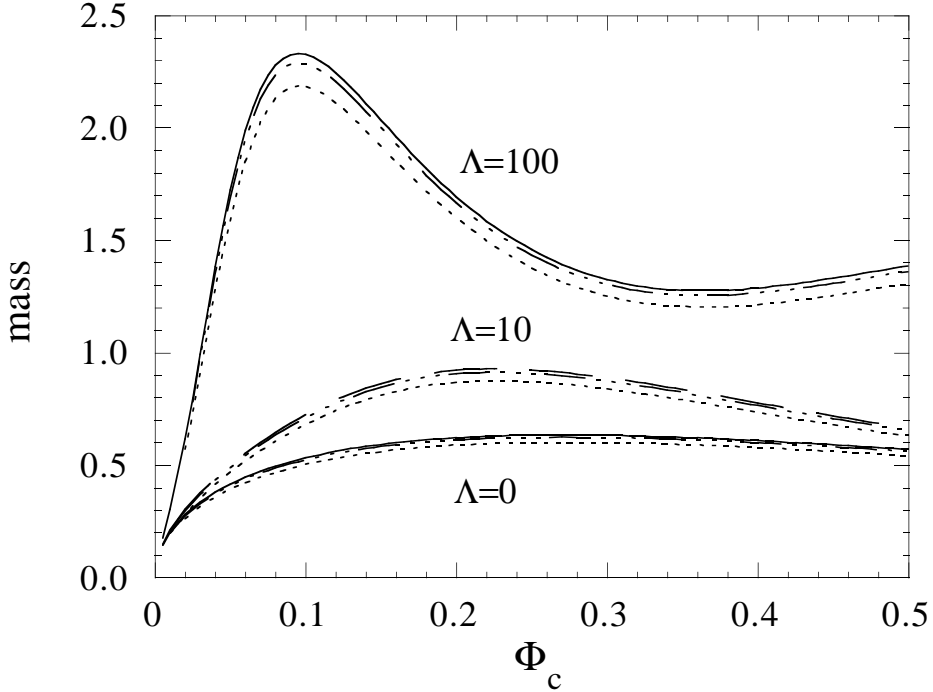


FIG. 10. Changing the boundary condition for  $\varphi_\infty$  via the cosmological solution of the quadratic coupling. The sequences of equilibrium solutions for cosmological time parameter  $p = 10$ (solid line), 6(three-dots-dash line) and 5(dotted line) are plotted. The solid lines are identical with those in Fig.5.

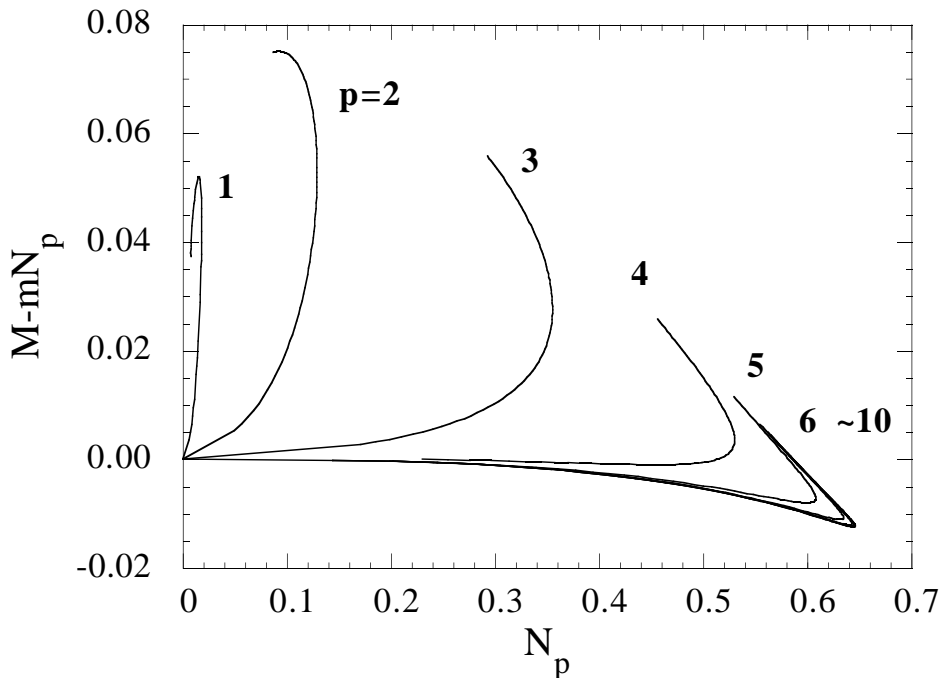


FIG. 11. Binding energy vs. particle number  $N_p$  for different cosmological time  $p = 10, 9, \dots, 1$ . The case for  $p = 10$  is the same as Fig.6. Only the range  $0 \leq \Phi_c \leq 0.5$  is plotted.